Polarization-entanglement-conserving frequency conversion of photons

S. Ramelow,[1,2] A. Fedrizzi,[2,*] A. Poppe,[1,3] N. K. Langford,[1,2,†] and A. Zeilinger[1,2]
[1]*Vienna Center for Quantum Science and Technology (VCQ), Faculty of Physics, University of Vienna, Boltzmanngasse 5, A-1090 Vienna, Austria*
[2]*Institute for Quantum Optics and Quantum Information, Austrian Academy of Sciences, Boltzmanngasse 3, A-1090 Vienna, Austria*
[3]*Austrian Institute of Technology (AIT), Donau-City-Straße 1, A-1220 Vienna, Austria*
(Received 9 June 2011; published 30 January 2012)

Entangled photons play a pivotal role in the distribution of quantum information in quantum networks. However, the frequency bands for optimal transmission and storage of photons are often not the same. Here, we experimentally demonstrate the coherent frequency conversion of photons entangled in their polarization, a widely used degree of freedom in photonic quantum information processing. We verify the successful entanglement conversion by violating a Clauser-Horne-Shimony-Holt (CHSH) Bell inequality and fully characterize our near-perfect entanglement transfer using both state and process tomography. Our implementation is robust and flexible, making it a practical building block for future quantum networks.

DOI: 10.1103/PhysRevA.85.013845 PACS number(s): 42.65.Ky, 03.67.Bg, 03.65.Wj, 42.50.Ex

I. INTRODUCTION

Quantum frequency conversion of single photons offers an elegant way to avoid the often difficult trade-offs associated with choosing one wavelength which is optimal for all parts of a connected quantum system. Quantum networks [1], for example, will facilitate the large-scale deployment of secure quantum communication [2]. They require the distribution of entanglement using flying qubits (photons) between quantum repeater nodes, which can coherently store entanglement in quantum memories and concatenate it by entanglement swapping [3]. However, the standard wavelength for optical fiber transmission is 1550 nm, where loss is minimized, whereas the highest efficiencies for coherent optical memories suitable for quantum information applications have to date been achieved in rubidium vapor at around 800 nm [4]. Such issues also arise in many other contexts, connected with, for example, detector performance (for 1550-nm photons), general transmission and dispersion properties of materials used, or the availability of suitable laser sources. Coherent frequency conversion of flying qubits can sidestep this type of problem altogether.

The basic process underlying optical frequency conversion is nonlinear sum frequency generation (SFG), where a pump and an input field are combined in a nonlinear medium to generate an output field with the sum of the input frequencies. A major experimental motivation for this has been to solve the detection problem for telecom-band single photons by converting them to the visible regime and using, instead of InGaAs-based photodetectors, the better-performing silicon detectors [5–8]. In the single-photon regime, where the input field is much weaker than the pump, near-100% conversion efficiencies can be achieved by optimizing interaction nonlinearities (e.g., by using waveguides [7,8]) or by using high pump intensities (e.g., with cavities [5] or pulsed pump lasers [6]). Critically, the SFG process can also conserve the quantum properties of the input light [9] and fulfill the fundamental requirements for universal photonic quantum interfaces: first, the conversion process must preserve the photons' indistinguishability [10,11] and single-photon character [12]; second, it must also preserve quantum information, and in particular entanglement, stored in the photons. Polarization entanglement is widely used in an array of quantum optics applications because of the remarkable precision and ease with which it can be generated, controlled, and measured. While phase- and polarization-maintaining conversion has been shown for classical fields [13–15] and conservation of entanglement has been reported for time-bin-entangled photons [16], entanglement-preserving conversion in the widely used and easily controlled polarization degree of freedom has so far only been achieved with highly narrowband photons using four-wave mixing in cold Rb vapor in high-vacuum environments [17].

Here, we demonstrate coherent conversion of polarization-entangled photons in an architecture that is compatible with integrated photonics technology by using a compact, robust, and simple design based on bulk crystal nonlinearities and off-the-shelf components. We stringently verified the entanglement transfer by violating a Clauser-Horne-Shimony-Holt (CHSH) [18] Bell inequality and fully characterized the near-perfect entanglement conversion using quantum state and process tomography. Coherent single-photon frequency conversion which preserves polarization entanglement will be a key enabling step for future quantum optical technologies, and devices like ours with flexible wavelength tuning and robust designs will be critical to making these practical in any realistic scenario.

II. SETUP

In our experiment (Fig. 1), the polarization-coherent up-conversion takes place in two orthogonally oriented, periodically poled $KTiOPO_4$ (ppKTP) crystals. The crystals are designed for type I quasi-phase-matching for 810 nm 1550 nm → 532 nm and oriented such that the horizontally (H) polarized component of the input at 810 nm is converted to

*Present address: ARC Centre for Engineered Quantum Systems, ARC Centre for Quantum Computation and Communication Technology, School of Mathematics and Physics, University of Queensland, Brisbane 4072, Australia.
†Present address: Department of Physics, Royal Holloway, University of London, Egham Hill, Egham TW20 0EX, United Kingdom.

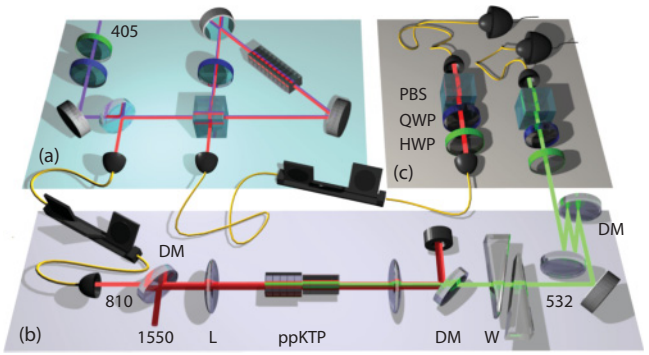

FIG. 1. (Color online) Experimental scheme. (a) Polarization-entangled photon source. Photon pairs are created by spontaneous parametric down-conversion in a periodically poled $KTiOPO_4$ (ppKTP) crystal, which is bidirectionally pumped by a 405-nm diode laser in a polarization-Sagnac loop [19,20]. (b) Polarization-coherent up-conversion setup. Signal (810 nm) and pump (1550 nm) are combined with a dichroic mirror (DM) and focused into the setup with a lens (L) of $f = 50$ mm. The two polarization components of the input are up-converted to 532 nm in one of two 4.3-mm-long, orthogonally oriented ppKTP crystals. The remaining 810-nm photons and 1550-nm pump light are separated from the 532-nm photons with dichroic mirrors: one in transmission and two in a z configuration for multiple reflections. Two adjustable calcite wedges (W) compensate temporal walk-off. (c) The polarization analysis (and preparation for the process tomography) is implemented with a quarter-wave plate (QWP), half-wave plate (HWP), and a polarizing element (PBS). The 532-nm photons are then coupled into a single-mode fiber and detected by a silicon avalanche photo-diode (Si-APD). The coincidences with the second 810-nm photon are identified by home-built coincidence logic.

532 nm in the first crystal, and the vertical (V) component is converted in the second. The crystals are placed close to each other to maximize conversion efficiency as well as stability and to minimize potential sources of mode distinguishability, which would decrease the polarization coherence. Chromatic dispersion and crystal birefringence cause a combined temporal walk-off of ∼1.8 ps between the orthogonal polarization components, similar to the photon coherence time [20]. To render the output photons indistinguishable, we compensate this walk-off with a pair of birefringent $CaCO_3$ (calcite) wedges with a combined thickness of ∼3 mm. Thus, an input state $\phi^+_{\text{in}} = (|H_{810}H_{810}\rangle + |V_{810}V_{810}\rangle)/\sqrt{2}$ is converted into:

$$\psi_{\text{out}} = \eta_H |H_{810}H_{532}\rangle + e^{-i\theta}\eta_V |V_{810}V_{532}\rangle. \tag{1}$$

The phase θ as well as the relative conversion efficiency η_H/η_V between the two crystals can be controlled through the polarization state of the 1550-nm photon laser beam, which we adjust with fiber-polarization controllers. The pump laser system consists of a tunable, fiber-coupled external-cavity diode laser amplified to 1 W with a high-power erbium-doped fiber amplifier. The pump field and the entangled photons were combined with a dichroic mirror and focused to spot sizes of ∼70 μm (1550) and ∼50 μm (810). After recollimation, the 532-nm light was separated from both the 1550-nm pump and the 810-nm photons via multiple reflections off three dichroic mirrors, suppressing the unconverted 810-nm photons by at least 100 dB. The up-converted 532-nm photon and its entangled 810-nm partner photon were then subjected to polarization analysis and detected by single-photon avalanche photo diodes, with a detection efficiency of around 50% both at 532 and 810 nm.

III. RESULTS

In our experiment, the optical conversion bandwidth—an important parameter in frequency conversion setups—is determined by the phase-matching properties and the length of the crystals used. The 4.3-mm-long ppKTP crystals provide an up-conversion bandwidth for the 810-nm photons of 410-GHz FWHM (0.9 nm). By comparison, the spectral bandwidth of photons used in the experiment was 250-GHz FWHM (0.55 nm), well below this, thus preventing any significant reduction of the conversion efficiency.

The conversion efficiency of this setup for Gaussian beams is theoretically given by [5]:

$$\begin{aligned} \eta &= \sin^2(\pi/2\sqrt{P_p/P_{\max}}), \\ P_{\max} &= \frac{c\epsilon_0 n_1 n_2 \lambda_1 \lambda_2 \lambda_p}{128 d_{\text{eff}}^2 L h_m}, \end{aligned} \tag{2}$$

with pump beam power P_p, input and output wavelengths $\lambda_{1,2}$, the corresponding crystal refractive indices $n_{1,2}$, the effective nonlinearity d_{eff}, crystal length L, and the focusing factor h_m (for Gaussian beams). The spot sizes of ∼70 μm (1550) and ∼50 μm (810), corresponding to a focusing parameter $\xi = \frac{L}{2z_R}$ (with Rayleigh length z_R) of about 0.8 for both beams, yield $h_m \sim 0.6$. For the maximally available pump power of 1 W and a single 4.3-mm-long crystal, we thus expect an efficiency of ∼0.8%. Experimentally, calibration measurements with a 810-nm laser diode resulted in 270 nW of 532-nm light converted from an input of 28 μW at 810 nm. Accounting for the wavelength difference and ∼16% optical loss, this implies an observed up-conversion efficiency of ∼0.6%. The discrepancy between theory and measurement is likely due to a slightly lower effective nonlinear coefficient caused by imperfect periodic poling.

For polarization-coherent operation, we convert one photon of an entangled (810 nm, 810 nm) pair in the ϕ^+ state created by our entangled photon source. From 7.3×10^4 counts per second (cps) input photon pairs, we detected 15 cps pairs after conversion, yielding an effective up-conversion efficiency of $\sim 2 \times 10^{-4}$. Considering fiber-coupling losses of 50%, this corresponds to an intrinsic conversion efficiency—directly after the crystals—of about 0.04%. After accounting for the reduction by 50% because each crystal is pumped at half the pump power and another ∼82% because the beam focus is located between the two crystals instead of the crystal centers, this number is in good agreement to the theoretical efficiency—primarily limited by available pump power—and our auxiliary laser diode measurements.

A stringent way to demonstrate that polarization entanglement is preserved in the conversion process is the violation of a Bell inequality [21], in our case the CHSH inequality [18] for the converted, (532 nm, 810 nm) polarization state:

$$S = E(\alpha,\beta) - E(\alpha,\beta') + E(\alpha',\beta) + E(\alpha',\beta') \leqslant 2, \tag{3}$$

where $E(\cdot,\cdot)$ are the correlations for joint polarization measurements on two photons along the angles $\alpha = 0°, \alpha' = 45°, \beta = 22.5°, \beta' = 67.5°$. A Bell value above the classical bound of 2 implies that the measured state is incompatible with a local realistic model [18,21] and is thus entangled. With about 15 cps coincidence rate and integrating over 100 s for each measurement, we recorded the coincidences for the 16 combinations of measurement angles, which includes the combinations with the additional 4 angles rotated by 90 deg from the above-mentioned angles, which is necessary to evaluate the Bell parameter when using only one detector on each side with polarization filters. We obtained an experimental Bell parameter of

$$S_{\text{exp}} = 2.615 \pm 0.027, \tag{4}$$

which violates the classical bound by more than 20 standard deviations. The observation of entanglement in the output state is striking, because the original 810-nm photon has been annihilated and created again in the 532-nm mode—a rather invasive interaction.

To assess the quantum nature of the up-conversion process, we characterized it using tomographic techniques. We first performed process tomography [22,23] with a strongly attenuated laser diode to assess the *intrinsic* (i.e., independent of imperfect detector performance) dynamics of the entanglement transfer. We prepared the input states $\{|H\rangle, |V\rangle, |D\rangle, |A\rangle, |R\rangle, |L\rangle\}$ and, for each input, measured the same set of six observables for the up-converted 532-nm single-photon output, where $|D\rangle = (|H\rangle + |V\rangle)/\sqrt{2}$, $|A\rangle = (|H\rangle - |V\rangle)/\sqrt{2}$, $|R\rangle = (|H\rangle + i|V\rangle)/\sqrt{2}$, and $|L\rangle = (|H\rangle - i|V\rangle)/\sqrt{2}$. According to Eq. (1), for $\theta = 0$ and balanced conversion, $\eta_H = \eta_V$, the ideal process matrix χ_{ideal} has a single nonzero element (I, I) in the Pauli-basis representation. This is very close to the reconstructed process matrix (Fig. 2), which has a process fidelity [24] to the ideal case of $\mathcal{F} = 99.23 \pm 0.01\%$. This indicates that the conversion process has excellent polarization coherence.

We subsequently characterized in detail the entanglement transfer, performing two-qubit quantum state tomography [24] on both the entangled photon input state and the entangled photon output state and comparing the two (see Fig. 3). For this,

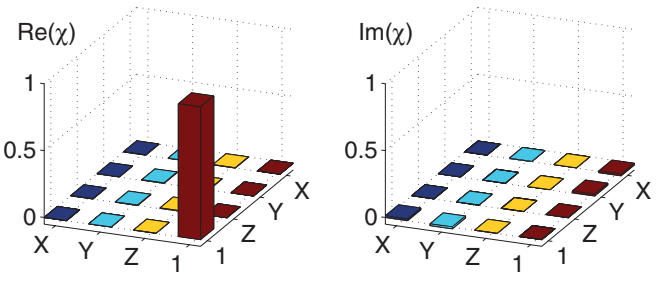

FIG. 2. (Color online) Process matrix χ (Pauli-basis representation) for polarization-coherent up-conversion, characterized by an attenuated 810-nm diode laser. The different elements of χ access what kind of operation—decomposed into the Pauli operations—an input state is subject to, with the dominating element denoting the identity operation. The calculated process fidelity $\mathcal{F}$ and purity (P) are $\mathcal{F} = 99.23 \pm 0.01\%$ and $\mathcal{P} = 98.54 \pm 0.01\%$. Error margins for $\mathcal{F}$ and (P) are determined assuming Poissonian count statistics.

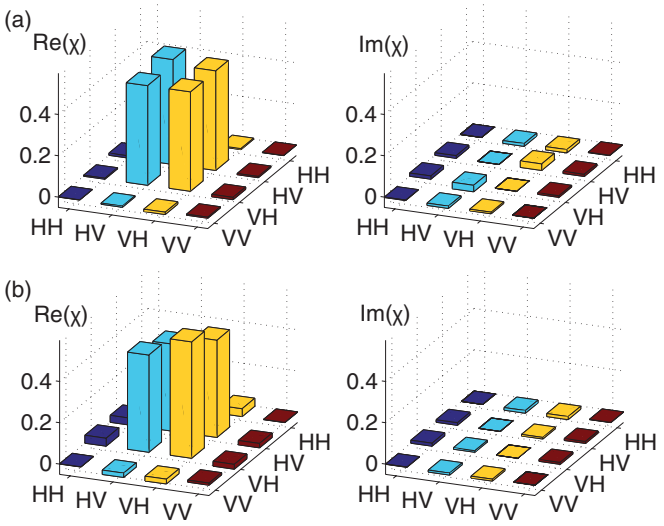

FIG. 3. (Color online) Reconstructed (accidental-corrected) two-qubit density matrices of entangled input states and output states. (a) Input state (810 nm, 810 nm) with a corresponding fidelity with respect to the ψ^+ state of $\mathcal{F}_{\text{in}} = 97.93 \pm 0.03\%$. (b) Output state (810 nm, 532 nm) with $\mathcal{F}_{\text{out}} = 96.7 \pm 0.2\%$. The fidelities as well as the values for the purities $(\mathcal{P})$ and tangles $(\mathcal{T})$ of the input and output states are summarized in Fig. 4. Error margins follow from Monte-Carlo simulations assuming errors assuming Poissonian count statistics.

we measured a total of 36 combinations of the 6 single-qubit observables $\{|H\rangle, |V\rangle, |D\rangle, |A\rangle, |R\rangle, |L\rangle\}$ for a measurement time of 1 s for the (810 nm, 810 nm) polarization-entangled input state and 100 s for the (810 nm, 532 nm) output state in which the first 810-nm photon remained unchanged. We used maximum-likelihood optimization to reconstruct the two-qubit density matrices from these measurements and calculated several key diagnostic parameters: the input state fidelity (with the maximally entangled Bell state ϕ^+) is $\mathcal{F}_{\rho_{\text{in}}} = 95.91 \pm 0.04\%$ and tangle is $\mathcal{T}_{\rho_{\text{in}}} = 84.3 \pm 0.1\%$. These values decrease to $\mathcal{F}_{\rho_{\text{out}}} = 93.8 \pm 0.3\%$ and $\mathcal{T}_{\rho_{\text{out}}} = 77 \pm 1\%$ for the (partially) up-converted states.

An error analysis shows that the most significant error contribution for both tomographic and Bell test results was caused by accidental coincidence counts, which occur when two photons from unrelated pairs are recorded within the coincidence time window. These cannot be fully distinguished from the correlated pairs, because the limited timing resolution of the single-photon detectors (≈1 ns) is much longer than the photon's coherence time (≈3 ps). However, compared with the total coincidence count rate, the accidental count rates were much lower, reaching comparable levels only for the polarization combinations exhibiting minima in the coincidences due to the high-fidelity entanglement. Note that this is itself an indication of the high quality of the polarization-preserving process. We did not observe any statistically significant pump-induced background counts. We estimated the accidental coincidence rates for every input and output measurement configuration by splitting one of the detector signals and measuring the coincidences with an additional relative time delay between the channels. We now subtract these accidentals from the raw coincidence counts in

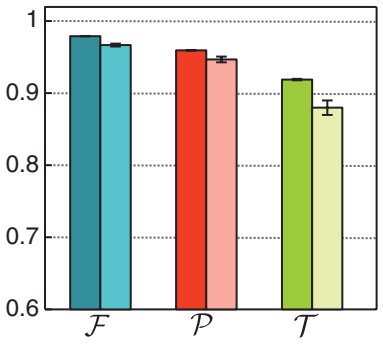

FIG. 4. (Color online) Summary of the quality parameters for the accidental-corrected input states ρ_{in} (dark) and output states ρ_{out} (light): fidelities $\mathcal{F}$, purities $\mathcal{P}$, and tangle $\mathcal{T}$. Error bars were obtained from Monte-Carlo runs of the tomographic reconstruction with assumed Poissonian count statistics.

reconstructing our output states to probe the intrinsic quality of the up-conversion process.

The resulting density matrices are shown in Fig. 3. The parameters for the corrected output states are $\mathcal{F}_{\rho_{\text{out}}} = 96.7 \pm 0.2\%$, $\mathcal{P}_{\psi_{\text{out}}} = 94.7 \pm 0.4\%$, and $\mathcal{T}_{\rho_{\text{out}}} = 88 \pm 1\%$. These and the corresponding values calculated from the accidental-corrected (as explained above) input state are summarized in Fig. 4. The exceptional quality of the polarization entanglement transfer is further highlighted by the overlap fidelity between the entangled input and output states of $\mathcal{F}_{\rho_{\text{in}},\rho_{\text{out}}} = 97.8 \pm 0.4\%$.

IV. CONCLUSIONS

To conclude, we have shown and verified the conversion of polarization entanglement with intrinsically near-unity fidelity using quantum state and process tomography. We furthermore violated a Bell inequality for the converted state. Our setup is flexible, compact, and robust; it uses simple bulk nonlinear materials, requires no cryogenic or vacuum apparatus, and is compatible with standard integrated-fiber and waveguide technologies. It is thus well suited for large-scale deployment in quantum networks and other quantum technologies where wavelength conversion is essential. Our conversion efficiencies are close to the theoretically calculated limit imposed by the available pump power and can be straightforwardly enhanced by known techniques to achieve near-unity single-photon efficiencies [5–8]. Specifically, for our polarization coherent design the efficiency can be significantly increased by using longer crystals and moving to bidirectionally pumped schemes (e.g., Sagnac- or Michelson-type interferometers [14]). Importantly, with pump schemes like ours where the pump has a lower frequency then the converted photons [25,26], the conversion can remain free of pump-induced noise even at the required high pump power.

Converting 810 nm to 532 nm, as demonstrated here, can be important for various reasons; for example, custom 532-nm single-photon detectors can have up to 10 times lower timing jitter than their 810-nm counterparts and superconducting nanowire detectors as well as imaging systems based charge-coupled device (CCD) cameras are more efficient at shorter wavelengths. The quasi-phase-matched interaction allows very flexible wavelength tuning (by temperature tuning of the crystal or adjusting the pump wavelength). Moreover, the wavelengths in our setup are interchangeable. Up-converting 1550-nm photons can be achieved by pumping with 810 nm, where powerful lasers are readily available. Coherent frequency conversion also opens up avenues in fundamental physics, such as enabling access to superposition bases for color qubits [27]. Finally, a future interesting challenge will be to change the photons' spectral bandwidth during frequency conversion via suitably designed phase matching similar to what has been proposed in Ref. [28]. This could prove useful for interfacing photons with narrow-bandwidth quantum memories.

ACKNOWLEDGMENTS

We thank M. Hentschel and T. Jennewein for valuable discussions. This work has been supported by the Austrian Science Fund within SFB 015 P06, P20, and CoQuS (W1210), by the ERC (Advanced Grant QIT4QAD), and by the European Commission Project QESSENCE.

[1] L. Duan, M. D. Lukin, J. I. Cirac, and P. Zoller, Nature (London) **414**, 413 (2001).
[2] V. Scarani, H. Bechmann-Pasquinucci, N. J. Cerf, M. Duscaronek, N. Lütkenhaus, and M. Peev, Rev. Mod. Phys. **81**, 1301 (2009).
[3] J. W. Pan, D. Bouwmeester, H. Weinfurter, and A. Zeilinger, Phys. Rev. Lett. **80**, 3891 (1998).
[4] M. Hosseini, B. Sparkes, G. Campbell, P. Lam, and B. Buchler, Nat. Commun. **2**, 174 (2011).
[5] M. Albota and F. Wong, Opt. Lett. **29**, 1449 (2004).
[6] A. P. VanDevender and P. G. Kwiat, J. Mod. Opt. **51**, 1433 (2004).
[7] C. Langrock, E. Diamanti, R. Roussev, Y. Yamamoto, M. Fejer, and H. Takesue, Opt. Lett. **30**, 1725 (2005).
[8] R. Thew, S. Tanzilli, L. Krainer, S. Zeller, A. Rochas, I. Rech, S. Cova, H. Zbinden, and N. Gisin, New J. Phys. **8**, 32 (2006).
[9] P. Kumar, Opt. Lett. **15**, 1476 (1990).
[10] H. Takesue, Phys. Rev. Lett. **101**, 173901 (2008).
[11] K. A. O'Donnell and A. B. U'Ren, Phys. Rev. Lett. **103**, 123602 (2009).
[12] M. T. Rakher, L. Ma, O. Slattery, X. Tang, and K. Srinivasan, Nat. Photonics **4**, 786 (2010).
[13] G. Giorgi, P. Mataloni, and F. DeMartini, Phys. Rev. Lett. **90**, 027902 (2003).
[14] M. A. Albota, F. N. C. Wong, and J. H. Shapiro, J. Opt. Soc. Am. B **23**, 918 (2006).
[15] A. P. VanDevender and P. G. Kwiat, J. Opt. Soc. Am. B **24**, 295 (2007).
[16] S. Tanzilli, W. Tittel, M. Halder, O. Alibart, P. Baldi, N. Gisin, and H. Zbinden, Nature (London) **437**, 116 (2005).
[17] Y. O. Dudin, A. G. Radnaev, R. Zhao, J. Z. Blumoff, T. A. B. Kennedy, and A. Kuzmich, Phys. Rev. Lett. **105**, 260502 (2010).

[18] J. F. Clauser, M. A. Horne, A. Shimony, and R. A. Holt, Phys. Rev. Lett. **23**, 880 (1969).
[19] T. Kim, M. Fiorentino, and F. N. C. Wong, Phys. Rev. A **73**, 012316 (2006).
[20] A. Fedrizzi, T. Herbst, A. Poppe, T. Jennewein, and A. Zeilinger, Opt. Express **15**, 15377 (2007).
[21] J. S. Bell, in *Physics*, Vol. 1 (Physics Publishing, New York, 1964), p. 195.
[22] J. F. Poyatos, J. I. Cirac, and P. Zoller, Phys. Rev. Lett. **78**, 390 (1997).
[23] I. L. Chuang and M. A. Nielsen, J. Mod. Opt. **44**, 2455 (1997).
[24] D. F. V. James, P. G. Kwiat, W. J. Munro, and A. G. White, Phys. Rev. A **64**, 052312 (2001).
[25] H. Dong, H. Pan, Y. Li, E. Wu, and H. Zeng, Appl. Phys. Lett. **93**, 071101 (2008).
[26] H. Kamada, M. Asobe, T. Honjo, H. Takesue, Y. Tokura, Y. Nishida, O. Tadanaga, and H. Miyazawa, Opt. Lett. **33**, 639 (2008).
[27] S. Ramelow, L. Ratschbacher, A. Fedrizzi, N. K. Langford, and A. Zeilinger, Phys. Rev. Lett. **103**, 253601 (2009).
[28] D. Kielpinski, J. F. Corney, and H. M. Wiseman, Phys. Rev. Lett. **106**, 130501 (2011).